Detoxification of organophosphates using imidazole-coated Ag, Au and AgAu nanoparticles†

Valmir B. Silva,[a] Thenner S. Rodrigues, [ID] [b] Pedro H. C. Camargo [ID] [b] and Elisa S. Orth [ID] *[a]

Organophosphate (**OP**) detoxification is a worldwide problem due to the high stability of P−O bonds. Here, we designed several imidazole-coated nanocatalysts targeted towards the cleavage of **OP** and thus their detoxification. Specifically, Ag, Au and bimetallic AgAu nanoparticles (NPs) supported on SiO$_2$ were functionalized with methimazole (**MTZ**), which comprises thiol and imidazole groups, foreseeing enabling freely available imidazole groups. Raman analyses indicate that **MTZ** interacts preferably *via* its sulfur atom over Au NPs and *via* the nitrogen of the imidazole ring over Ag NPs. The **MTZ**-derived nanocatalysts were effective towards **OP** cleavage. For instance, rate enhancements of 10^8 fold were obtained for the toxic pesticide **Paraoxon**, compared to the uncatalyzed reaction. Interestingly, Au-derived nanocatalysts were significantly more effective since the imidazole group is free to react with the **OP**, which is not possible when Ag−N interactions take place.

Introduction

Organophosphates (**OP**) are intrinsically related to many fundamental biological functions, such as biosynthesis, signaling, regulation, and energy transduction.[1] Moreover, they are responsible for the preservation of genetic information since they constitute DNA and RNA strands.[2] Actually, one-third of all biological proteins are phosphorylated at some time, evidencing the importance of phosphoryl transfer. **OP** are mostly known for their high stability.[3] For example, the hydrolysis of DNA is estimated take in over 100 000 years.[4] Since enzymes are very successful in promoting phosphorylation in biological systems,[2] they have bioinspired many mimicking studies. The downside of **OP**'s stability is that they have been used as a scaffold for many chemical warfare and pesticides (Scheme 1), knowingly to have high toxicity, sometimes even being lethal.[5] Not surprising, much effort has been directed towards the development of efficient methods of destruction and detection of these toxic **OP**, focusing on deactivating unused (probably prohibited) stockpiles and monitoring abusive use of agrochemical and/or chemical attacks[5,6]

It is noteworthy that poisoning by pesticides is a serious worldwide public concern.[7] As a matter of security, many studies in this field have used structural mimics of pesticides and chemical warfare that usually have lower toxicity and higher reactivity so that the reaction can be feasibly followed. For example, dimethyl methylphosphonate (**DMMP**), *p*-nitrophenyl diphenylphosphate (**PNPDPP**),[5] and diethyl-2,4-dinitrophenyl phosphate (**DEDNPP**)[8–10] have been explored, as shown in Scheme 1.

In order to pursue the detoxification of **OP**, many bio-inspired models have been proposed as detoxifying agent or artificial enzymes targeting the phosphoryl cleavage.[5] In this context, imidazole-derived catalysts have attracted great
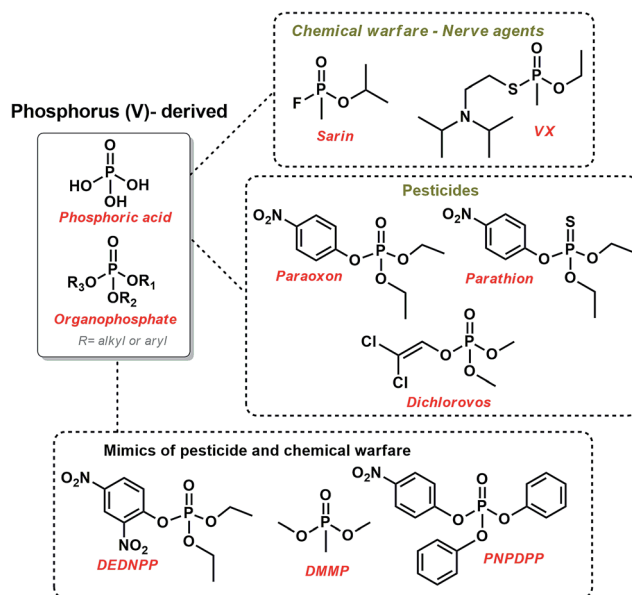
Scheme 1 The structure of some relevant organophosphates used as chemical warfare and pesticides, along with some mimics of toxic **OP**.

[a]*Departamento de Química, Universidade Federal do Paraná, CP 19032, 81531-980 Curitiba, PR, Brazil. E-mail: elisaorth@ufpr.br*

[b]*Instituto de Química, Departamento de Química Fundamental, Universidade de São Paulo, Av. Prof. Lineu Prestes 748, SP 05508-900, São Paulo, Brazil*

† Electronic supplementary information (ESI) available. See DOI: 10.1039/c7ra07059d
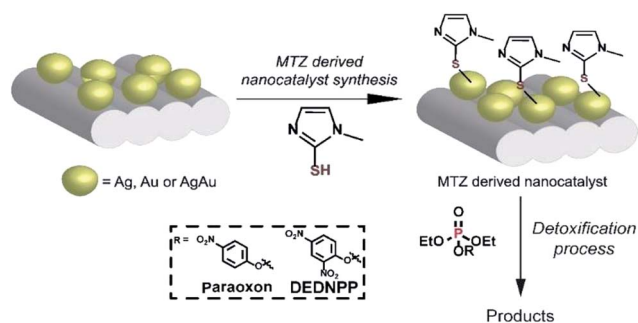
Fig. 1 Functionalization of AuSiO$_2$, AgSiO$_2$ or AgAuSiO$_2$ with MTZ.

attention due to their presence in many enzymatic active sites and their chemical versatility,[11] *i.e.*, they can react as acid–base or nucleophilic catalysts under considerably mild conditions (pH ~ 7).[12,13] Another promising class of catalysts for **OP** cleavage involve nanoparticles (NPs),[14] although there are still only a few reports in this field,[5,15–20] in contrast to the many studies regarding NPs-based sensors for various **OP**.[21]

The physicochemical features of several NPs, such as shape and size, can be decisive for catalysis.[22–24] A previous study showed that the reduction of 4-nitrophenol can be catalyzed by Ag and AgAu NPs alone, with higher reactivity for the later attributed to Au content and the increased surface area due to the hollow interiors.[25] In another study, bimetallic nanoshells of AgAu, AgPd, and AgPt NPs were used as bio-metallo catalysts with dual activity for transesterification; and silane oxidation.[26] Insofar, to the best of our knowledge, there are no studies correlating NPs features with its effect on **OP** degradation.

Herein, we coated silver (**AgSiO$_2$**), gold (**AuSiO$_2$**) and bimetallic nanoshells **AgAuSiO$_2$** NPs (supported on SiO$_2$) with a thiol-substituted imidazole (methimazole, **MTZ**) in order to obtain nanocatalysts with freely available imidazole moieties. We choose **MTZ** due to the extraordinary catalytic activity known for imidazole groups (*vide supra*) and the thiol group that interacts favorably with NPs,[20,27] hence anchoring efficiently imidazole moieties on the NPs surface. For this purpose, the NPs were firstly obtained with controlled shape and size following a previously reported procedure.[28,29] Then, the NPs were functionalized with **MTZ** (Fig. 1). Finally, the nanocatalysts were evaluated toward **OP** degradation, using the simulant **DEDNPP** and the pesticide **Paraoxon** as model substrates.

Experimental

Materials

MTZ Analytical grade silver nitrate (AgNO$_3$, 99%, Sigma-Aldrich), polyvinylpyrrolidone (PVP, Sigma-Aldrich, M.W. 10 000 g mol^{-1}), polyvinylpyrrolidone (PVP, Sigma-Aldrich, M.W. 55 000 g mol^{-1}), ethylene glycol (EG, 99.8%, Sigma-Aldrich), tetrachloroauric(III) acid trihydrate (HAuCl$_4$·3H$_2$O, ≥99.9%, Sigma-Aldrich), silica (pore size 22 Å, 800 m^2 g^{-1}, CAS number 112926-00-8, Sigma-Aldrich), ethanol (Êxodo) were used as received.

Synthesis of Ag NPs[29]

Ag seeds were prepared by the polyol process. In a typical experiment, 5 g of polyvinylpyrrolidone (PVP, 10 000 g mol^{-1}) was dissolved in 37.5 mL of ethylene glycol. Then, AgNO$_3$ (200 mg, 1.2 mmol) was added and mixed until the complete dissolution. The resulting solution was heated to 125 °C for 2.5 hours, leading to the appearance of a greenish-yellow color, allowed to cool down to room temperature, and diluted to 125 mL of water. After this step, 46 mL of the resulting suspension (0.2197 mg mL^{-1}, determined by ICP) were washed twice with ethanol and three times with water by successive rounds of centrifugation at 15 000 rpm and removal of the supernatant. After washing, the product was suspended in 10 mL of deionized water.

Synthesis of Au NPs[30]

The synthesis of Au nanospheres was performed by a seeded growth approach. In the first step, Au seeds were synthesized by adding 150 mL of a 2.2 mmol L^{-1} sodium citrate aqueous solution to a 250 mL round-bottom flask under magnetic stirring. This system was heated to 100 °C for 15 minutes. Then, 1 mL of a 25 mmol L^{-1} AuCl$_4^-$(aq) solution was added, and the reaction mixture was kept at 100 °C under vigorous stirring for 30 minutes. The obtained Au nanoparticles were employed as seeds for the synthesis of Au NPs having larger sizes by two successive steps of Au deposition. For the first deposition step, 1 mL of a 60 mmol L^{-1} sodium citrate solution was added to the same 250 mL round-bottom flask containing the Au NPs seeds under magnetic stirring at 100 °C for 5 minutes. Afterward, 1 mL of a 25 mmol L^{-1} AuCl$_4^-$(aq) solution was added to the reaction mixture containing the Au NPs seeds and the reaction mixture was carried out for another 30 min. Similarly, a second deposition step could be performed by adding another 1 mL of a 60 mmol L^{-1} sodium citrate solution and 1 mL of a 25 mmol L^{-1} AuCl$_4^-$(aq) solution to the reaction mixture obtained after the first deposition step, in which the Au NPs produced after the first deposition step served as seeds for further growth. After the reaction, the resulting suspension was allowed to cool down to room temperature. After this step, 88 mL of the resulting suspension (0.1146 mg mL^{-1}, determined by ICP) were washed three times with water by successive rounds of centrifugation at 15 000 rpm and removal of the supernatant. After washing, the product was suspended in 10 mL of deionized water.

Synthesis of AgAu nanoshells[29]

The synthesis of AgAu nanoshells was based on the galvanic replacement reaction between Ag nanospheres and AuCl$_4^-$(aq). In a typical procedure, a mixture containing 50 mL of PVP aqueous solution (0.1 wt%, M.W. 55 000 g mol^{-1}) and 10 mL of the as-prepared suspension containing the Ag nanospheres was stirred at 100 °C for 10 min in a 250 mL round-bottom flask. Then, 20 mL of AuCl$_4^-$(aq) (0.6 mmol L^{-1}) was added dropwise and the reaction allowed to proceed at 100 °C for another 1 h. After that, the suspension was allowed to cool down to room temperature and 28 mL (0.0458 mg mL^{-1}, determined by ICP)

were washed twice with a supersaturated NaCl solution and three times with water by successive rounds of centrifugation at 15 000 rpm and removal of the supernatant. After washing, the product was suspended in 10 mL of deionized water.

Synthesis of the SiO₂ supported NPs[28]

The incorporation of Ag, Au, and AgAu nanostructures onto a silica matrix (1% wt, metal basis) were performed based on a wet impregnation approach. In a typical run, 10 mL of the suspensions containing the respective nanoparticles washed and concentrated were added dropwise to a beaker containing 1 g of commercial silica suspended in 20 mL of deionized water under magnetic stirring. The resulting mixture was stirred at room temperature for 24 h. After this step, the resulting suspensions were washed three times with distilled water and twice with ethanol by successive rounds of centrifugation at 7000 rpm and removal of the supernatant. The resulting catalysts were then treated at 120 °C for 2 h under air.

Coating of the NPs with MTZ

The **MTZ** derived nanocatalysts were prepared as follows: 500 mg of the SiO₂ supported **AgSiO₂**, **AuSiO₂** or **AgAuSiO₂** NPs was added to a becker along with **MTZ** (26.0, 15.0 and 21.0 mg for **AgSiO₂**, **AuSiO₂** and **AgAuSiO₂**, respectively) in 50 mL of ethanol. The mixture was stirred during 24 h followed by centrifugation (12 000 rpm) and separated. In the following, the material was washed with ethanol (three times), centrifuged, and the supernatant was discarded. The ethanol was evaporated at room temperature. The samples were denominated **AgSiO₂–MTZ**, **AuSiO₂–MTZ** and **AgAuSiO₂–MTZ**, originated from **AgSiO₂**, **AuSiO₂**, and **AgAuSiO₂** NPs, respectively.

Characterizations

For the NPs, the scanning electron microscopy (SEM) images were obtained using a JEOL field emission gun electron microscope JSM6330F operated at 5 kV. The samples were prepared by drop-casting an aqueous suspension containing the nanostructures over a silicon wafer, followed by drying under ambient conditions. Transmission electron microscopy (TEM) images were obtained with a JEOL JEM1010 microscope operated at 80 kV. Samples for TEM were prepared by drop-casting an aqueous suspension of the nanostructures over a carbon-coated copper grid, followed by drying under ambient conditions. UV-vis spectra were obtained from aqueous suspensions containing the nanostructures with a Shimadzu UV-1700 spectrophotometer. The Ag and Au atomic percentages were measured by inductively coupled plasma optical emission spectrometry (ICP-OES) using a Spectro Arcos equipment. The X-ray diffraction (XRD) data were obtained using a Rigaku-Miniflex equipment, CuKα radiation. The diffraction pattern was measured in the range of 10–90° 2θ with a 1° min⁻¹ angular speed scan. For the **MTZ**-derived NPs, Raman spectra were obtained with a Renishaw spectrophotometer using the 632.8 nm excitation laser, with 25 accumulations and 25–50% of the laser intensity.
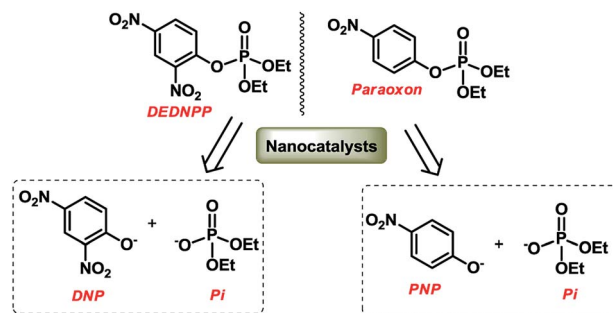
Scheme 2 Cleavage reaction of **DEDNPP** and **Paraoxon** in the presence of the nanocatalysts.

Catalytic studies of OP detoxification

For the catalytic studies, two **OP** were employed: **DEDNPP** and **Paraoxon**. Pseudo-first order conditions were maintained, where 30 mg of **MTZ**-derived nanocatalyst was added to 3 mL of a buffered solution (bicarbonate 0.2 mol L⁻¹). The reaction started upon addition of 15 μL of **DEDNPP** or **Paraoxon** stock solution (5×10^{-3} mol L⁻¹ in acetonitrile) and the medium was maintained under magnetic stirring (4 h and 15 days for **DEDNPP** and **Paraoxon**, respectively). The suspension was centrifuged (12 000 rpm) and UV-vis spectra of the supernatant were recorded. The catalytic activity was calculated based on the product concentration, hence **OP** degradation by measuring the absorbance variation at 400 nm related to the products 4-nitrophenolate (**PNP**) or 2,4 dinitrophenolate (**DNP**), that originated from **Paraoxon** and **DEDNPP**, respectively (Scheme 2). The molar absorptivity (ε) used were 18 380 and 12 100 L mol⁻¹ cm⁻¹ for **PNP** and **DNP**, respectively.[31,32] Considering pseudo-first order kinetics, already corroborated for these reactions in a separate study, the integrated rate law was used to obtain the pseudo-first order constant.
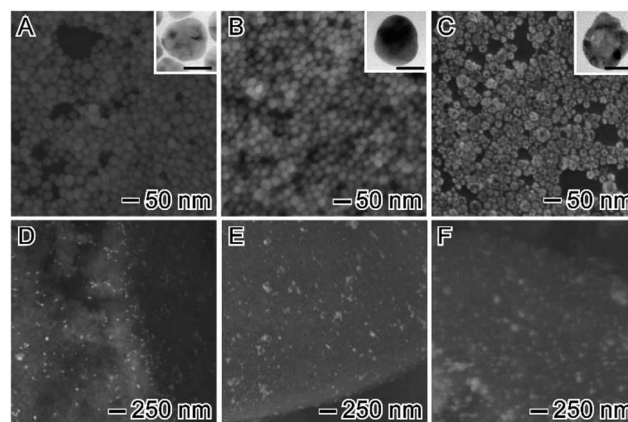

Fig. 2 (A–C) SEM images of Ag nanospheres (A), Au nanospheres (B), and AgAu nanoshells (C). The insets correspond to their corresponding TEM images (the scale bars in the insets correspond to 20 nm). (D–F) SEM images of (D) **AgSiO₂**, (E) **AuSiO₂**, and (F) **AgAuSiO₂** materials that were obtained from wet impregnation of the samples (A–C) onto a commercial SiO₂ support.

Results and discussion

Characterization of the SiO₂ supported NPs

Our studies started with the synthesis of Ag nanospheres, Au nanospheres, and AgAu nanoshells as shown in Fig. 2A–C, respectively. Ag nanospheres (Fig. 2A) were obtained by a one-step polyol approach and were 35 ± 4 nm in diameter.[33] On the other hand, Au nanospheres (Fig. 2B) were obtained by a seeded growth approach, in which Au nanospheres obtained by citrate reduction of AuCl₄⁻(aq) acted as template for additional Au deposition and growth leading to the formation of nanoparticles displaying larger diameters (36 ± 3 nm) that were similar to the Ag nanospheres.[30] For the AgAu nanoshells, the obtained Ag nanospheres were employed as sacrificial templates in the galvanic replacement reaction using AuCl₄⁻(aq), which represents an effective strategy for the synthesis of hollow nanostructures displaying controllable properties in a single-step.[29,34] As depicted in Fig. 2C, the formation of the hollow interiors is confirmed by the brighter mass-thickness contrast at the center of the AgAu nanoshells, which were 36 ± 4 nm in diameter, in agreement with the use of Ag nanospheres as templates. Interestingly, all obtained nanostructures displayed spherical shapes and relatively monodisperse sizes, which allowed us systematically investigate their catalytic performances as a function of the compositions and structures. The metal at% in the nanostructures were determined by ICP-OES analyses and corresponded to 100% of Ag, 100% of Au, and 49% of Ag + 51% of Au for Ag, Au, and AgAu, respectively.

After the synthesis of the Ag, Au, and AgAu nanostructures, we turned our attention to their incorporation onto the surface of a commercial SiO₂ in order to produce powdered catalysts, which are strongly desired in terms of heterogeneous catalysis due to their relatively easy separation, purification, and reuse. In addition, the uniform incorporation of NPs over solid supports have also been demonstrated as a promising strategy to prevent the particle agglomeration during the catalytic processes.[28] Fig. 2D–F show SEM images for the produced catalysts after the NPs incorporation onto the SiO₂ support. Interestingly, for all nanomaterials, an excellent dispersion of metal constituents was

Fig. 3 UV-vis extinction spectra recorded from aqueous suspensions containing Ag nanospheres (black trace), Au nanospheres (red trace), and AgAu nanoshells (blue trace).
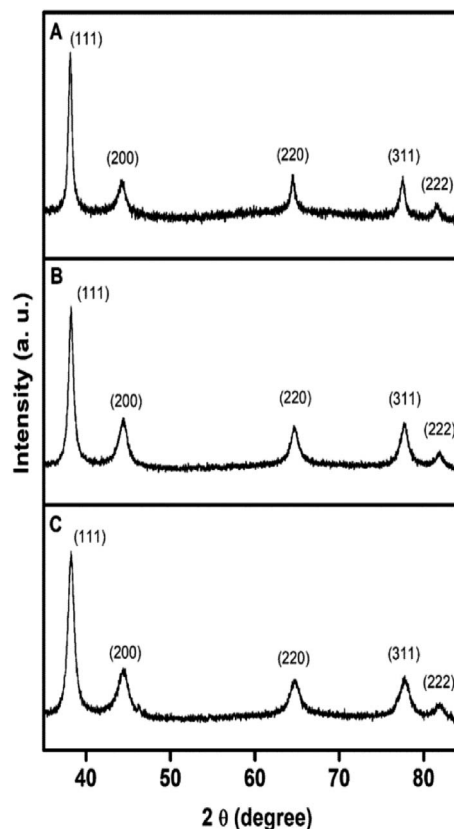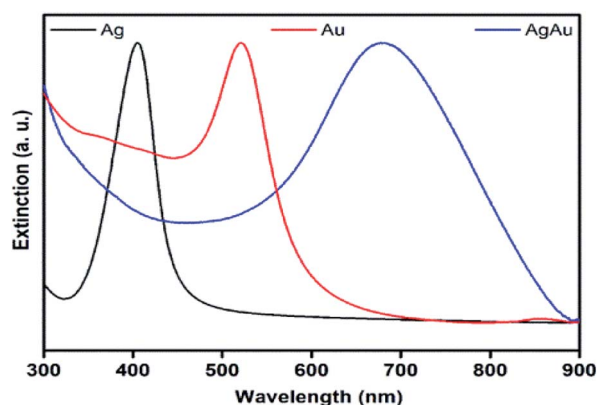

Fig. 4 XRD profiles of (A) Ag nanospheres, (B) Au nanospheres, and (C) AgAu nanoshells.

observed over the entire SiO₂ surface and no significant agglomeration and changes on the morphologies were detected, indicating the robustness of our employed wet impregnation method to produce solid metal/SiO₂ catalysts. Here, the metal loading corresponded to 1 wt% (Fig. 2F). The solid catalysts were denoted **AgSiO₂** (Fig. 2D), **AuSiO₂** (Fig. 2E), and **AgAuSiO₂**.

Fig. 3 shows the UV-vis extinction spectra for the obtained Ag and Au nanospheres and AgAu nanoshells. The Ag and Au nanospheres displayed clear extinction peaks centered at ≈ 410 and 520 nm assigned to the dipolar mode of their surface plasmon resonance excitation[29,30] On the other hand, a red-shift and broadening of the SPR in the AgAu nanoshells was observed compared to the Ag nanospheres employed as templates. This behavior can be associated with the Au deposition as well as the formation of the hollow interiors in during the galvanic reaction.[25]

The formation of Ag, Au, and AgAu was also monitored by XRD analyses (Fig. 4), in which the XRD patterns also confirmed the formation of Ag (Fig. 4A), Au (Fig. 4B) and AgAu (Fig. 4C) nanostructures without the presence of any significant crystalline impurities. However, as both Ag and Au has very similar lattice constants, the XRD diffraction peaks for these two species could not be resolved under our experimental conditions.

Characterization of the MTZ-derived NPs coated material

Regarding the **MTZ**-derived NPs, to the best of our knowledge, this represents the first report using **MTZ** on NPs supported on
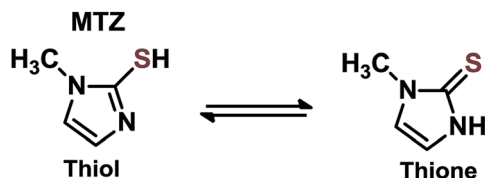
Scheme 3 Tautomeric equilibrium for MTZ.

SiO₂. There are other studies that report other thiol-substituted imidazole for coating NPs, evidencing that the thiol group interacts with the NPs, enabling freely available imidazole moieties. For example, in a previous study, authors report a dipeptide-functionalized thiol with terminal histidine and carboxylate groups that was used to passivate Au NPs. The material was successfully prepared and used as catalysts in acyl transfer reactions, although the NPs nature was not the focus of study.[27] In another report, *N*-methylimidazole derivative functionalized Au NPs were obtained similarly *via* thiol anchoring on NPs surface, which afterward was employed in the cleavage of 2,4-dinitrophenyl acetate.[20] It is noteworthy, that we also attempted to anchor **MTZ** on NPs (Ag, Au, and AgAu) not supported on SiO₂, but functionalization was followed by aggregation of the particles.

MTZ is a known drug (commercially Tapazol) used for the treatment of hyperthyroidism.[35] **MTZ** has a tautomeric equilibrium of thiol–thione as shown in Scheme 3. The concentration of each species depends on the pH, although in general, the thione species predominates. For example, at pH 9, the percentage of thione is 65%.[36] Another important feature of **MTZ** is its pK_a of 11.38.[35]

The **MTZ**-derived NPs were characterized by Raman spectroscopy. Indeed, Raman analysis of **MTZ** is quite difficult due to its tautomeric and ionic equilibrium, but overall results evidence that the NPs were successfully functionalized. Raman spectra are presented in Fig. 5 including spectrum of pure **MTZ** for comparison and additionally all spectra all plotted together in Fig. S1.† The Raman spectra for the NPs prior to the **MTZ** functionalization (red trace on Fig. 5) show bands that were characteristic of PVP (in the case of **AgSiO₂** and **AgAuSiO₂**), citrate (in the case of **AuSiO₂**) and SiO₂ (spectra for pure SiO₂ and PVP are shown in the ESI†).[37,38] These species are present at the surface of the NPs as they were employed as stabilizers during the synthesis of each respective material. It is important to note that all the nanoparticles were washed by successive rounds of centrifugation and removal of the supernatant after their synthesis and isolation, material. Although this process removes the reducing agents, unreacted precursors, and the excess of stabilizers that are employed during the synthesis, stabilizer molecules remain at the surface of the NPs. Their detection in the Raman experiments is due to the surface-enhanced Raman scattering (SERS) effect as enabled by Ag, Au, and AgAu NPs.

Upon functionalization (**AgAuSiO₂–MTZ**, **AgSiO₂–MTZ** and **AuSiO₂–MTZ** in Fig. 5) it is possible identify some characteristic bands of **MTZ** that are identified in the first spectrum:[17,35,36] (i) at
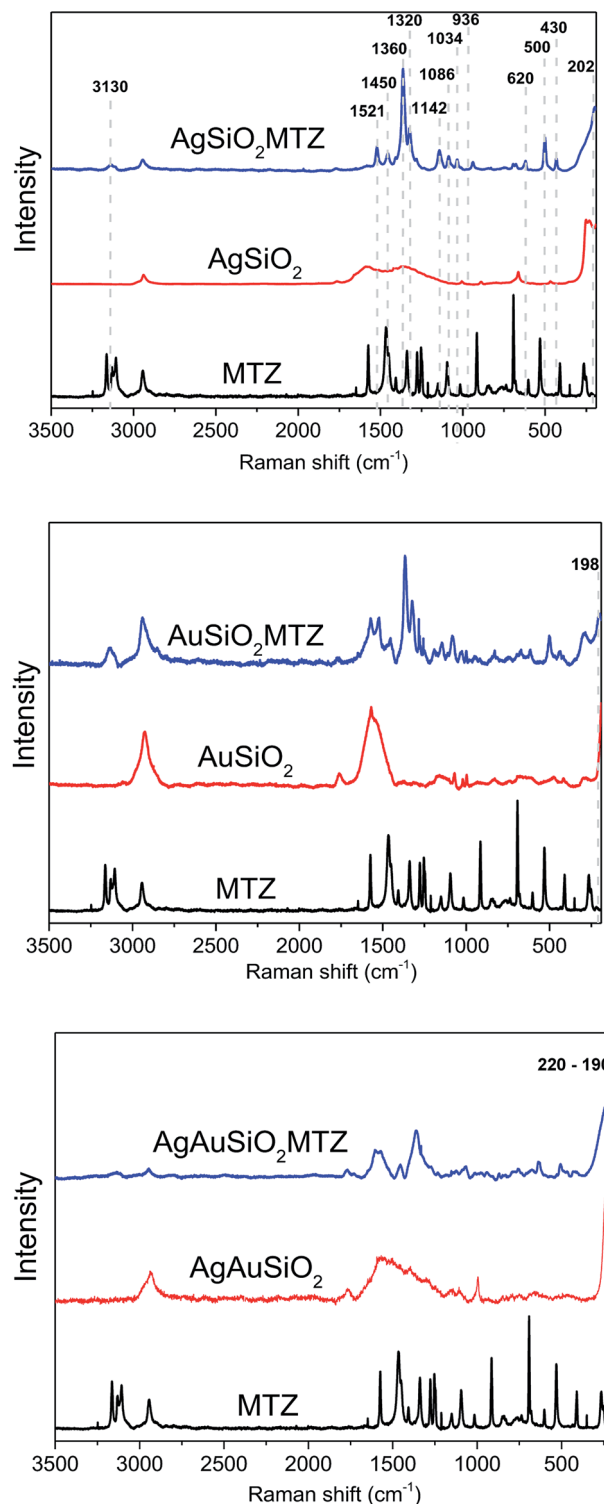
Fig. 5 Ordinary Raman and SERS spectra ($l = 632.8$ nm) for pure **MTZ**, bare NPs, and **MTZ**-functionalized Ag, Au and AgAu NPs.

3130 cm⁻¹ due to ring C–H stretching; (ii) at 1521 cm⁻¹ due to C–C and C–N stretching, along with ring C–H bending; (iii) at 1450 cm⁻¹ attributed to C–S and ring C–N stretching, in addition to ring C–H bending; (iv) at 1360 cm⁻¹ (most intense band) referent to C–N ring stretching with contribution of C–H

bending; (v) at 1320 cm^{-1} attributed to ring C–N stretching, ring bending and ring CH–NH bending; (vi) 1142 cm^{-1} referent to C–S and ring C–N stretching, along with ring C–H bending; (vii) at 1086 cm^{-1} due to ring C–N stretching and ring C–H bending; (viii) at 1034 cm^{-1} attributed to ring bending, ring C–H bending, methylene C–H bending (ix) at 936 cm^{-1} referent to ring bending, ring C–N stretching and ring CH–NH bending; (x) at 620 cm^{-1} due to out-of-plane ring and CH–NH bending; (xi) at 500 and 430 cm^{-1} due to out-of-plane ring bending. It is noticeable that spectrum for pure **MTZ** presents more bands than discussed above and in addition some bands of **MTZ** are shifted when comparing coated materials to pure **MTZ**. Actually, these detected differences for the SERS spectra from the functionalized materials and ordinary Raman from pure **MTZ** are characteristic of many molecules and indicate that the functionalization was successful as previously observed.[35,36,39] Moreover, the bands observed herein indicate that **MTZ** is present as thione and thiol/thiolate,[35,36] although it should be noted that despite the high pK_a for **MTZ**, previous studies show that the thiolate species is preferable for interacting with Ag and Au NPs.[35]

Regarding the nature of the interaction between NPs and **MTZ**, previous studies report that **MTZ** interacts with Au NPs preferably *via* the thiol group.[35] On the other hand, with Ag NPs, there are some reports that claim a preferable interaction *via* the nitrogen atom of the imidazole group,[36] although another study evidences that Ag NPs can also interact with thiol group[35] or with both groups concomitantly.[39] In fact, when analyzing Raman spectrum for **AuSiO$_2$–MTZ**, there is a band at 198 cm^{-1}, not present in the non-coated material. Despite the typical bands of SiO$_2$ in this region, they don't seem to overlap. This new band has been attributed in the literature to Au–S stretching, indicating that for this material, **MTZ** interacts preferably *via* the thiolate group.[35] In the case of **AgSiO$_2$–MTZ**, the band at 202 cm^{-1}, inexistent without **MTZ**, can be attributed to Ag–N stretching,[36] indicating that for this material **MTZ** interacts preferably *via* the imidazole ring through the lone pair of the nitrogen atom. Finally, for **AgAuSiO$_2$–MTZ,** the spectrum is noisier, with a broad band in the region of 220–190 cm^{-1} that could be attributed to both Ag–S and Au–N interactions.

It should be noted that despite the similarities in the bands attributed to Au–S and Ag–N, the other possible interactions Au–N and Ag–S are known to occur at higher wavenumbers (Au–N $\sim$225 cm^{-1} and Ag–S $\sim$240 cm^{-1}).[40,41] Taken together, Raman analysis confirms that **MTZ** was anchored on the NPs and that for **AuSiO$_2$–MTZ** the interaction seems to occur through the imidazole ring (Ag–N). For **AgSiO$_2$–MTZ**, this occurs *via* the thiolate group (Au–S). For **AgAuSiO$_2$–MTZ**, there could be a combination of these interactions. In addition, the following catalytic studies agree with the interaction proposed since due to the lower catalytic activity of **AgSiO$_2$–MTZ**.

FTIR analyses were also carried out (shown in ESI†) but didn't show any evident differences, probably due to the low degree of functionalization and also to the known low intensity of the bands of imidazole and thiol moieties. The **MTZ** molecule is only detected by Raman spectroscopy as a result of the SERS effect. Due to the low amount of metal ($\sim$1% in mass) and given
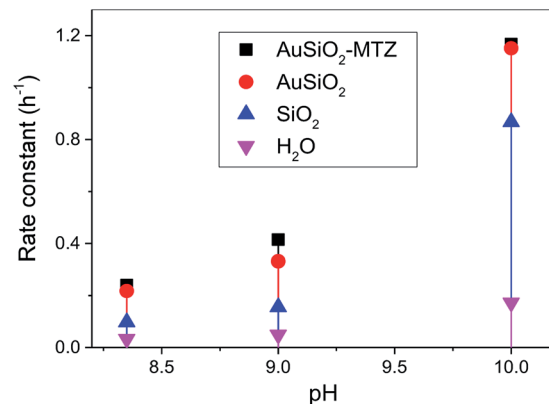

Fig. 6 pH effect rate constant for the reaction of Au-derived NPs with **DEDNPP** at 20 °C. Reaction with SiO$_2$ and in water is shown for comparison.[42]

that the **MTZ** is anchored solely on the nanoparticle, the overall amount of **MTZ** is extremely low to detect or differentiate by FTIR.

Catalytic activity on the detoxification of OP

The catalytic activity of the **MTZ**-derived materials was evaluated in the cleavage reactions of **OP**, thus its detoxification. Firstly, as a proof-of-concept, we choose one class of material, derived from Au, to react with the model **OP** (*i.e.* simulant) **DEDNPP**. This is a common strategy before applying with real life **OP** due to their higher toxicity. In addition, **DEDNPP** is more reactive than **Paraoxon**, hence its reaction can be followed on a shorter time scale. Upon confirmation of the catalytic activity with **DEDNPP**, the nanocatalysts are then evaluated in the reaction with **Paraoxon**. Fig. 6 presents the rate constants at different pH values for the cleavage of **DEDNPP** with **AuSiO$_2$**-derived catalysts. Constants solely with SiO$_2$ under the same conditions is also shown along with the reaction in water (spontaneous).[42,43]

Firstly, it should be noted that reactions with solely **MTZ** is not shown, since its comparison is not straightforward because of its homogenous reaction nature (herein is heterogeneous) and to the difficulty of estimating the amount of **MTZ** coating the NPs. Therefore we cannot obtain the rate constant of pure **MTZ** in the same concentration coating the NPs, hence would lead to erroneous underestimated comparison. In addition, we could not evaluate the reactions of bare NPs since they aggregate. Results show that **AuSiO$_2$–MTZ** is, in fact, effective in cleaving **DEDNPP**, specially at pH 9.0, since it differentiates from the non-coated material (**AuSiO$_2$**). At lower pH, the **MTZ**-derived material shouldn't exhibit any activity due to the lower reactivity of imidazole moiety.[42] On the other hand, at pH 10, the reaction is very effective in all cases due to the contribution of the alkaline hydrolysis (reaction in water). Reactions solely with SiO$_2$ evidenced for pH 8 and 9, similar constants to the spontaneous reaction, although at pH 10, its higher activity can be attributed to hydroxide species on the surface.[44] Insofar, the pH of interest to carry out further studies with the pesticide was

Table 1 Rate constants for the cleavage reaction of **Paraoxon** with the nanocatalysts[a]

	Rate constant, g^{-1} h^{-1}
AgAuSiO$_2$	4.10
AgSiO$_2$	4.03
AuSiO$_2$	4.58
AgAuSiO$_2$–MTZ	13.10
AgSiO$_2$–MTZ	3.76
AuSiO$_2$–MTZ	9.52

[a] pH 9.0, 20 °C. Rate constants are given as a function of the mass of metal in the nanocatalysts. Reactions solely with SiO$_2$, where similar to the analogous spontaneous reaction at pH 9.0.

9.0, since the **MTZ**-derived material showed higher reactivity (although discrete) than their non-functionalized analogous.

Considering the positive results with **DEDNPP**, the nanocatalysts were then evaluated in the reactions with the highly toxic pesticide **Paraoxon** at pH 9. Table 1 presents the rate constants obtained given as a function of the mass of metal for the reactions of **Paraoxon** with all the materials: coated and non-coated with **MTZ**. In general, catalytic rate constants are given as a function of the reactive group of the catalysts, although in this case, it was not possible to calculate the concentration of **MTZ** in the materials obtained, low values are expected. One approach is to obtain the ratio of the rate constants and the total amount of catalysts, but since in the present study it was impregnated with SiO$_2$, we found more convenient to consider the amount of metal that is responsible for interacting with the **MTZ** molecules. Nevertheless, not all NPs surface may be covered by **MTZ**, hence the rate constant considering solely the amount of **MTZ** reacting should be even higher. Overall, Table 1 evidences high rate constants for **Paraoxon** were among the highest reported in the literature. For example, previous studies with thiol-based nanocatalysts derived from graphene oxide show rate constants of 2.13 g^{-1} h^{-1} (considering the amount of the reactive group thiolate) with **Paraoxon**.[10] In another study, Ag, and cobalt (Co) NPs were coated with imidazole derived fatty acids that give rate constants for Co-derived material ~1.3 g^{-1} h^{-1} (considering the amount of metal).[16] A magnetic nanocatalyst of iron oxide with supported amino acids (Asp–His) was also used to cleave **Paraoxon** with a rate constant of 0.30 g^{-1} h^{-1} (considering the amount of Fe$_2$O$_3$–Asp–His).[18]

While only discrete enhancements were observed for the **MTZ**-derived materials towards **DEDNPP** in comparison to its non-functionalized material, the difference was substantially different with **Paraoxon** (for Au- and AgAu-based materials). This is not unprecedented since **Paraoxon** is much less reactive than **DEDNPP**. In fact, as mentioned, **DEDNPP** is a simulant of **OP** such as **Paraoxon** and is used to verify possible catalytic effects, since the response is fast.

A more detailed analysis of Table 1 shows that upon functionalization of **AuSiO$_2$** with **MTZ**, the rate constant nearly doubles. In the case of **AgAuSiO$_2$**, the analogous **MTZ** nanocatalyst increases more significantly the rate constant. In
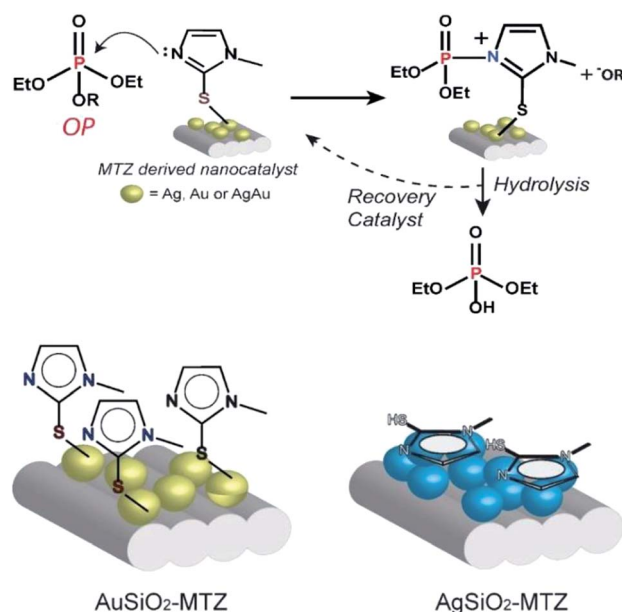

Fig. 7 The mechanism proposed for the reaction of the **OP** with the nanocatalysts and interaction of **MTZ** with Au and Ag-derived materials.

contrast, with **AgSiO$_2$**, functionalization slightly decreases the rate constant. This behavior agrees with previous Raman analyses that indicate that for Ag-derived materials, **MTZ** interacts *via* the nitrogen while Au-based materials prefer the sulfur atom. Hence, the effect of **MTZ** on Au- and AgAu-based nanocatalysts is different from that of Ag-based materials. This can be explained by the expected mechanism for reactions of imidazole with **OP**, shown in Fig. 7. Based on previous mechanistic studies,[45] the nitrogen of the imidazole ring attacks the phosphorus atom, thus cleaving the **OP** and leading to a phosphorylated intermediate and the phenolic product –OR. In the following, the unstable intermediate is hydrolyzed giving inorganic phosphate and regenerating the **MTZ**-derived nanocatalyst. This mechanism has been broadly accepted for imidazole mediated reactions and occurs analogously in many enzymatic active sites, therefore the nanocatalysts can be considered as artificial enzymes. Further, the proposed mechanism is consistent with the recycling of the nanocatalyst. Indeed, the UV-vis spectra taken after the reactions don't show any lixiviation of **MTZ** or the NPs, since the only band that appears in solution is of the products.

Correlating the mechanism with the proposed interaction for **AuSiO$_2$–MTZ** (or **AgAuSiO$_2$–MTZ**) and **AgSiO$_2$–MTZ** (vide Raman), we can observe that, while Au–S guarantees freely available imidazole groups, Ag–N, doesn't (shown in Fig. 7). Therefore, **AgSiO$_2$–MTZ** doesn't exhibit significant catalytic activity in contrast to **AuSiO$_2$** due to the type of interaction that directly disables the mechanistic preference.

Regarding the catalytic activity for the NPs without **MTZ**, this can be attributed to the Lewis acidity of the metal which interacts favorably with the phosphoryl oxygen, leading to a more electrophilic phosphorus center, as observed for ester cleavage (phosphate or acyl).[15,16]
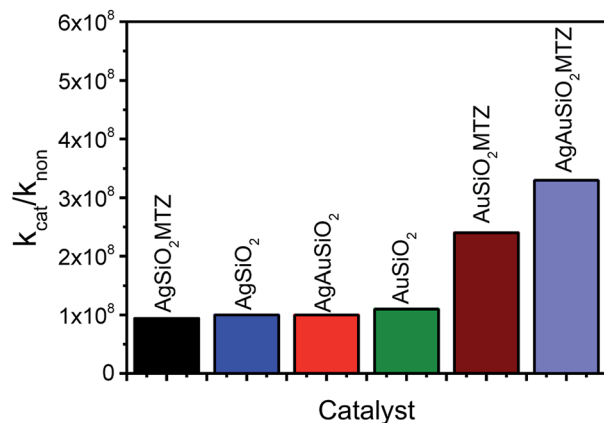
Fig. 8 Rate enhancements of the nanocatalysts with **Paraoxon** (k_{cat} in $g^{-1} h^{-1}$) compared to the reaction with water (k_{H_2O} in $g^{-1} h^{-1}$).[45]

Fig. 8 presents the rate enhancements of the nanocatalysts with **Paraoxon** when compared to its spontaneous reactions ($k_{H_2O} = 1.20 \times 10^{-7} h^{-1}$ or $4.0 \times 10^{-8} g^{-1} h^{-1}$),[45] evidencing that the materials proposed are highly reactive towards **OP** detoxification. Interestingly, **AgAuSiO$_2$–MTZ** is the most efficient nanocatalyst. This could be related to another previous study that concluded that bimetallic AgAu NPs (without SiO$_2$) are better catalysts toward 4-nitrophenol reduction than Au or Ag NPs. This effect was attributed to a possible higher surface area, resulting from the formation of porous/hollow walls.[25]

Conclusions

Herein, we functionalized Ag, Au and bimetallic AgAu NPs (supported on SiO$_2$) with **MTZ**, in order to obtain nanocatalysts comprising freely available imidazole groups. Results evidence that the NPs were successfully coated and that **MTZ** interacts preferably *via* sulfur atom over Au NPs and *via* the imidazole nitrogen over Ag NPs. The nanocatalysts were highly effective towards **OP** cleavage. For example, Fig. 9 illustrates the efficiency of detoxification of the toxic **OP Paraoxon** with the nanocatalysts, that is given as the time in days taken to degrade 50% of the **OP**. Normally in water, the lifetime of **Paraoxon** is extremely high and the estimated time to degrade 50% is over 600 years.[45] In the presence of the nanocatalysts, this time is reduced to 7 days with the most reactive **AgAuSiO$_2$–MTZ**.
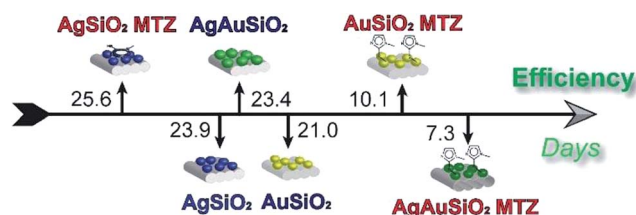

Fig. 9 Efficiency for the detoxification of **Paraoxon** by the nanocatalysts, given as the time in days required to degrade 50%.

The higher activity of Au-derived nanocatalysts was attributed to the imidazole group that is free to react with the **OP**, since in this case Au–S interactions is preferable. When Ag–N interactions takes place, the reactivity of imidazole is reduced.

Overall, we were able to detoxify **OP** efficiently which is promising destroying toxic stocks and also to design monitoring devices for these compounds. These perspectives are aligned with the importance of the issue as evidenced by the Peace Nobel Prize in 2013 awarded by the Organization for the Prohibition of Chemical Weapons "for its extensive efforts to eliminate chemical weapons".[46]

Conflicts of interest

There are no conflicts to declare.

Acknowledgements

References

1 S. C. L. Kamerlin, P. K. Sharma, R. B. Prasad and A. Warshel, *Q. Rev. Biophys.*, 2013, **46**, 1–132.

2 F. H. Westheimer, *Science*, 1987, **235**, 1173–1178.

3 A. J. Kirby, B. S. Souza and F. Nome, *Can. J. Chem.*, 2015, **93**, 422–427.

4 S. C. Kamerlin, P. K. Sharma, R. B. Prasad and A. Warshel, *Q. Rev. Biophys.*, 2013, **46**, 1.

5 K. Kim, O. G. Tsay, D. A. Atwood and D. G. Churchill, *Chem. Rev.*, 2011, **111**, 5345–5403.

6 Y. C. Yang, J. A. Baker and J. R. Ward, *Chem. Rev.*, 1992, **92**, 1729–1743.

7 R. T. Delfino, T. S. Ribeiro and J. D. Figueroa-Villar, *J. Braz. Chem. Soc.*, 2009, **20**, 407–428.

8 A. M. Manfredi, W. Demos, E. H. Wanderlind, B. V. Silva, A. C. Pinto, B. S. Souza and F. Nome, *J. Phys. Org. Chem.*, 2016, **29**, 600–603.

9 E. S. Orth, J. E. S. Fonsaca, T. G. Almeida, S. H. Domingues, J. G. L. Ferreira and A. J. G. Zarbin, *Chem. Commun.*, 2014, **50**, 9891–9894.

10 J. Fonsaca, L. Hostert, E. S. Orth and A. J. Zarbin, *J. Mater. Chem. A*, 2017, **5**, 9591–9603.

11 P. V. Attwood, M. J. Piggott, X. L. Zu and P. G. Besant, *Amino Acids*, 2007, **32**, 145–156.

12 K. Hofmann, *Imidazole and its derivatives*, Interscience Publishers, New York, 1953.

13 J. G. Ferreira and E. S. Orth, *J. Braz. Chem. Soc.*, 2017, **28**, 1760–1767.

14 P. Xu, S. Guo, H. Yu and X. Li, *Small*, 2014, **10**, 2404–2412.

15 M. H. Kuchma, C. B. Komanski, J. Colon, A. Teblum, A. E. Masunov, B. Alvarado, S. Babu, S. Seal, J. Summy and C. H. Baker, *Nanomedicine*, 2010, **6**, 738–744.

16 L. Bromberg, L. Chen, E. P. Chang, S. Wang and T. A. Hatton, *Chem. Mater.*, 2010, **22**, 5383–5391.

17 L. Bromberg and T. A. Hatton, *Ind. Eng. Chem. Res.*, 2007, **46**, 3296–3303.

18 Y. Zheng, C. Duanmu and Y. Gao, *Org. Lett.*, 2006, **8**, 3215–3217.

19 L. Y. Kuo, A. K. Bentley, Y. A. Shari'ati and C. P. Smith, *Organometallics*, 2012, **31**, 5294–5301.

20 L. Pasquato, F. Rancan, P. Scrimin, F. Mancin and C. Frigeri, *Chem. Commun.*, 2000, 2253–2254.

21 L. Rassaei, F. Marken, M. Sillanpää, M. Amiri, C. M. Cirtiu and M. Sillanpää, *TrAC, Trends Anal. Chem.*, 2011, **30**, 1704–1715.

22 J. Zeng, Q. Zhang, J. Chen and Y. Xia, *Nano Lett.*, 2009, **10**, 30–35.

23 C. Jin, J. Han, F. Chu, X. Wang and R. Guo, *Langmuir*, 2017, **33**, 4520–4527.

24 T. S. Rodrigues, A. G. da Silva, A. B. de Moura, I. G. Freitas and P. H. Camargo, *RSC Adv.*, 2016, **6**, 62286–62290.

25 M. V. Petri, R. A. Ando and P. H. Camargo, *Chem. Phys. Lett.*, 2012, **531**, 188–192.

26 C. M. Kisukuri, D. J. Palmeira, T. S. Rodrigues, P. H. Camargo and L. H. Andrade, *ChemCatChem*, 2016, **8**, 171–179.

27 P. Pengo, S. Polizzi, L. Pasquato and P. Scrimin, *J. Am. Chem. Soc.*, 2005, **127**, 1616–1617.

28 T. S. Rodrigues, A. H. da Silva, A. G. da Silva, D. G. Ceara, J. F. Gomes, J. M. Assaf and P. H. Camargo, *Catal. Sci. Technol.*, 2016, **6**, 2162–2170.

29 T. S. Rodrigues, A. G. da Silva, A. Macedo, B. W. Farini, R. d. S. Alves and P. H. Camargo, *J. Mater. Sci.*, 2015, **50**, 5620–5629.

30 A. G. da Silva, T. S. Rodrigues, A. Macedo, R. T. da Silva and P. H. Camargo, *Quim. Nova*, 2014, **37**, 1716–1720.

31 G. N. Bowers, R. B. McComb, R. Christensen and R. Schaffer, *Clin. Chem.*, 1980, **26**, 724–729.

32 L. J. Daumann, L. Marty, G. Schenk and L. R. Gahan, *Dalton Trans.*, 2013, **42**, 9574–9584.

33 K. TekaiaáElhsissen, *J. Mater. Chem.*, 1996, **6**, 573–577.

34 Y. Sun, B. Mayers and Y. Xia, *Adv. Mater.*, 2003, **15**, 641–646.

35 M. Muniz-Miranda, F. Muniz-Miranda and A. Pedone, *Phys. Chem. Chem. Phys.*, 2016, **18**, 5974–5980.

36 N. Biswas, S. Thomas, A. Sarkar, T. Mukherjee and S. Kapoor, *J. Phys. Chem. C*, 2009, **113**, 7091–7100.

37 D. De Faria, H. Gil and A. De Queiroz, *J. Mol. Struct.*, 1999, **478**, 93–98.

38 J. García-Aguilar, D. Cazorla-Amorós and Á. Berenguer-Murcia, *Appl. Catal., A*, 2017, **538**, 139–147.

39 T. A. Saleh, M. M. Al-Shalalfeh and A. A. Al-Saadi, *Sci. Rep.*, 2016, **6**, 32185.

40 B. Pergolese, M. Muniz-Miranda and A. Bigotto, *J. Phys. Chem. B*, 2004, **108**, 5698–5702.

41 P. Galinetto, A. Taglietti, L. Pasotti, P. Pallavicini, G. Dacarro, E. Giulotto and M. Grandi, *J. Appl. Spectrosc.*, 2016, **82**, 1052–1059.

42 E. S. Orth, E. H. Wanderlind, M. Medeiros, P. S. M. Oliveira, B. G. Vaz, M. N. Eberlin, A. J. Kirby and F. Nome, *J. Org. Chem.*, 2011, **76**, 8003–8008.

43 E. H. Wanderlind, Cinética e mecanismo de hidrólise do triéster dietil 2,4-dinitrofenil fosfato, Master thesis, Federal University of Santa Catarina, 2014.

44 A. Torrents and A. T. Stone, *Environ. Sci. Technol.*, 1991, **25**, 143–149.

45 E. S. Orth, T. G. Almeida, V. B. Silva, A. R. M. Oliveira, F. M. M. Ocampos and A. Barison, *J. Mol. Catal. A: Chem.*, 2015, **403**, 93–98.

46 https://www.nobelprize.org/nobel_prizes/peace/laureates/2013/opcw-facts.html, accessed in May, 5, 2017.